# Four-Point Bending Fatigue Behavior of Al$_2$O$_3$-ZrO$_2$ Ceramic Biocomposites Using CeO$_2$ as Dopant

*Maycol Moreira Coutinho[a]* [iD], *Anne Caroline de Paula Nascimento[a]* [iD],

*José Eduardo Vasconcelos Amarante[b], Claudinei dos Santos[c]** [iD], *Jorge Luiz de Almeida Ferreira[a]* [iD],

*Cosme Roberto Moreira da Silva[a]* [iD]

*[a]Universidade de Brasília, Faculdade de Tecnologia, Asa Norte, 70910-900, Brasília, DF, Brasil.*
*[b]Universidade Federal Fluminense, Rua Doutor Sílvio Henrique Braune, 22, 28625-650, Nova Friburgo, RJ, Brasil.*
*[c]Universidade do Estado do Rio de Janeiro, Faculdade de Tecnologia, Rod. Presidente Dutra, km 298, 27537-000, Resende, RJ, Brasil.*

This work investigated the effect of adding ceria-stabilized tetragonal zirconia (Ce-TZP) on the fatigue behavior of alumina-based ceramic composites. Alumina powder (control group) and mixtures containing 5 wt.% (group A) and 20 wt.% (group B) of a commercial *m*-ZrO$_2$/Al$_2$O$_3$/CeO$_2$ powder mixture were milled/homogenized, compacted, sintered at 1600°C-2h, and submitted to hydrothermal degradation. The samples were characterized by relative density, microstructure, crystalline phases, and static mechanical properties. The cyclic fatigue strength was determined using the modified staircase method in 4-point bending tests. The results indicate that adding the *m*-ZrO$_2$/Al$_2$O$_3$/CeO$_2$ powder mixture to the Al$_2$O$_3$-matrix increases the tetragonal-ZrO$_2$ grains (Ce-TZP) content, presenting 2.9 wt.% of Ce-TZP and 11.9 wt.% of Ce-TZP for group A and group B, respectively. Furthermore, the addition of Ce-TZP improves densification (98.5% → 99.1%) with a slight reduction in hardness and modulus of elasticity and a significant K$_{IC}$ increase of the composite (K$_{IC}$ = 6.7 MPa.m$^{1/2}$, group B) when compared to monolithic alumina (K$_{IC}$=2.4 MPa.m$^{1/2}$). The fatigue strength limit of the control group was around 100 MPa, while the composites (groups A and B) presented the values of 279 MPa and 239 MPa, respectively. The results indicated that the incorporation of Ce-TZP significantly improves the fracture toughness of alumina-based ceramics. On the other hand, regarding the fatigue behavior, there was an increase in fatigue resistance in group A, resulting from the benefits of the *t→m* Ce-TZP grains transformation, which occurs during cyclic loading, producing a zone shielding that involves the tip of the crack, slowing its growth. The increase in the amount of Ce-TZP (group B) leads to an increase in the internal residual stresses between the phases due to anisotropy and difference in the thermal expansion coefficients, which accelerates the phase transformation and formation of microcracks at grain boundaries, reducing the fatigue strength of composites of group B.

**Keywords:** *Zirconia-toughened alumina (ZTA), Ce-TZP reinforcement, fracture toughness, fatigue behavior, four-point tests, modified staircase method.*

## 1. Introduction

Structural bioceramics based on alumina (Al$_2$O$_3$) have high hardness and wear resistance, in addition to recognized thermo-mechanical stability and bio-inertia. On the other hand, this material is brittle and has low fracture toughness and mechanical strength[1-4]. These restrictions limit their applications in different areas, as they lack structural reliability. To improve its performance, incorporating a second ceramic phase allows the development of composites that enhance the lower properties of the alumina matrix. In this context, the composites of toughened alumina with tetragonal zirconia, ZTA[5,6], are presented as a viable alternative since both phases have thermal stability and biocompatibility.

Yttria-stabilized tetragonal zirconia (Y-TZP), and in particular, its variant stabilized with 3 mol. % of Y$_2$O$_3$ (3Y-TZP) is the primary dopant of Al$_2$O$_3$-based biocomposites because their mechanical properties, in particular, the fracture toughness are notably superior to monolithic alumina[7]. The considerable increase of K$_{IC}$ compared to monolithic-Al$_2$O$_3$ is attributed to the good dispersion of Y-TZP grains in the Al$_2$O$_3$-matrix, which acts as a second phase that activates a toughening mechanism by *tetragonal→ monoclinic (t→m)* phase transformation[8,9]. However, this material has a recognized[10] low resistance to hydrothermal degradation, limiting its use as a biomaterial in humid or aqueous environments, such as in oral environments or where body fluids predominate. Moreover, it can lead to medium- or long-term aging with

*e-mail: claudineisvr@gmail.com

considerable mechanical strength and reliability losses. Ceramics based on ceria-stabilized tetragonal zirconia (Ce-TZP) are an interesting alternative to the traditional 3Y-TZP. They have resistance to degradation and fracture toughness superior to 3Y-TZP due to the nature of the chemical configuration and the crystalline arrangement of the unit cells of tetragonal $ZrO_2$-grains, which are stabilized with $Ce^{4+}$ in place of $Y^{3+}$. Previous studies have shown[9,11] that Ce-TZP grains have higher shear stress and require increased free energy necessary for phase transformation. Consequently, during the growth and propagation of a crack around these grains, the shielding zone characteristic of the periphery of the crack tip is superior to the Y-TZP, guaranteeing to the material a higher energy requirement for the crack propagation, which results in the material toughness increase[12].

Recently, a new class of materials based on Ce-TZP reinforced with $Al_2O_3$[13-16] and/or hexaluminates (H6A)[17-20] has resulted in composites with very high fracture toughness, greater than 10 MPa.m$^{1/2}$. However, with low abrasion resistance or hardness values compared to pure alumina. On the other hand, few reports refer to Ce-TZP as $Al_2O_3$ reinforcement in studies investigating these composites' dynamic mechanical properties (fatigue). Due to the randomness of the fatigue phenomenon, a high number of tests are performed for safety. However, when there are limited samples, the modified staircase method is an option, using a smaller amount of specimens. Concerning other methods, the modified staircase method can reduce the number of samples by 30 to 40% since the process concentrates the tests on stresses close to the estimated average fatigue limit. Another advantage of the technique is the simplicity of the statistical analysis. The first test uses the modified staircase method, with stress below the previously estimated fatigue strength limit. Subsequent tests are defined based on the result of the previous test. If the specimen reaches a number of cycles ($Nc$) without failure, the run-out will have been reached. A stress increment is then added to the previous one. However, if the specimen fails, two stress increments are deducted from the stress at which the failure occurred. This increment is previously calculated, and it is recommended to be equal to, or less than 5% of the initially estimated fatigue limit[21-23].

In this method, the number of failures and run-outs are generally equal. However, one of the two may be less frequent than the other. To calculate the mean stress amplitude $\overline{\sigma_0}$ and the sample standard deviation, Equations 1 and 2 are used, respectively, distinguishing in the equation the cases in which C is equal to 1 or 2. The method uses only the least frequent occurrence in the test results. When the least recurring event is a failure, the equation with C = 1 is used. If the less frequent events are run-outs, use the equation with C = 2 [21].

$$\overline{\sigma_0} = \sigma_{0min} + d.\left(\frac{A}{F} - \frac{1}{2}\right), \text{ when C=1}$$

$$\overline{\sigma_0} = \sigma_{0min} + d.\left(\frac{A}{F} + \frac{1}{2}\right), \text{ when C=2} \qquad (1)$$

$$1.62.d.\left(\frac{F.B - A^2}{F^2} + 0.029\right) \qquad (2)$$

Where $\sigma_{0min}$ is the lowest stress level for the least frequent occurrence and d is the stress increment used. The values of F, A, and B are calculated according to Equations 3, 4 and 5, where $i$ is the number of stress levels that caused failures and $f_i$ is the number of samples that passed through this amplitude of tension.

$$F = \Sigma f_i \qquad (3)$$

$$A = \Sigma i f_i \qquad (4)$$

$$B = \Sigma i^2 f_i \qquad (5)$$

After calculating the sample mean and standard deviation, two conditions must be satisfied to validate the method. However, if any of the conditions are not met, it is recommended to repeat the test. Therefore, Equations 6 and 7 for validation are indicated.

$$\frac{BF - A^2}{F^2} > 0,3 \qquad (6)$$

$$0,5s < d < 1,5s \qquad (7)$$

It is necessary to guarantee the confidence that the value of the mean stress amplitude $\overline{\sigma_0}$ is above the chosen fatigue limit, using a confidence interval for the mean of the specimens. The value of $\overline{\sigma_0}$ follows the t-Student distribution, which is symmetric about the mean. In this way, it is possible to correct it to ensure with $X\%$ confidence that the mean of the fatigue limit of retests will be above this value. This statistically corrected mean value can be calculated by Equation 8, where $X\%$ is the desired confidence, and $n$ is the number of specimens[24,25].

$$\sigma_{0x\%} = \overline{\sigma_0} - t_{\alpha,n-1}\frac{s}{\sqrt{n}} \qquad (8)$$

In turn, the standard deviation corrected by the confidence of $X$ % has a chi-square distribution. In this case, the confidence level is used to ensure that new tests will have a standard deviation below the upper limit of the sample standard deviation statistically corrected by the chi-square distribution[26].

This other value of the statistically corrected standard deviation must be calculated by Equation 9, where the failure probability limits are taken into account[26]

$$s_{x\%} = \sqrt{\frac{n-1}{X_{a,n-1}^2}}.s \qquad (9)$$

There are few published studies on cyclic and static fatigue at room temperature for advanced ceramics. However, the fatigue test poses some problems. One of them is the high dispersion of results, which impairs the tendency to fatigue results. This dispersion is considered to come from the component's intrinsic parameters. Due to this scattering in results, it cannot yet be said that the theory of fatigue in ceramics is consolidated[27]. Jie Zhang and co-authors[28] investigated ceramics' microstructure and mechanical properties based on zirconia, alumina, and silicon carbide. Scherrer's et al. work[29] aimed to determine the fatigue

limits of 3Y-TZP composites and characterize the types of failure that affect the fatigue strength limit. In this case, different commercial dental zirconia-based materials were used, since the samples' polished surfaces presented a ZrO$_2$-monoclinic phase in addition to tetragonal, resulting from the $t \rightarrow m$ transformation induced by the polishing process. The fatigue tests showed that the polishing and the surface monoclinic transformation improves the fatigue resistance between 15 and 30%, but the aspects related to hydrothermal degradation were not investigated.

The objective of the present work was to investigate the effect of the incorporation of Ce-TZP grains on the static and dynamic mechanical performance of Alumina-based ceramic composites, with particular attention to studying the effects of different Ce-TZP doping on the 4-point fatigue strength of these ZTA composites.

## 2. Experimental Procedure

### 2.1. Processing

A commercial nanoparticles powder mixture (ZirPro® Intense (Saint Gobain, France) containing $m$-ZrO$_2$(64wt.%)-Al$_2$O$_3$(25wt.%)-CeO$_2$(11wt.%) previously mixed was added to the high-purity submicrometric Al$_2$O$_3$ powder (CT3000 LS) in different proportions. The main characteristics of the raw materials are presented in Table 1.

Three different ceramics were investigated in this work: monolithic-Al$_2$O$_3$ (control group) and Al$_2$O$_3$ mixtures containing 5 wt.% (Group A) and 20 wt.% (Group B) of ZrO$_2$-Al$_2$O$_3$-CeO$_2$ commercial mixture, herein designated Ce-ZTA. Mixtures of Al$_2$O$_3$ (CT3000) with Ce-ZTA powder were homogenized using high-energy milling (RETSCH PM100, Germany). The powders were wet-milled at 450 RPM for 60 minutes, using a 500 mL alumina jar and sintered alumina spheres (Ø10 mm). In all compositions, including pure alumina, 4 wt.% polyvinyl alcohol-based binder (0.04%) was added to aid compaction. Samples with final dimensions after sintering of 45 mm x 5 mm x 5 mm (n = 20/group) were uniaxially compacted, with double piston action, applying a maximum pressure of 100 MPa, for 60 s. These samples were sintered in an electric furnace (Nabertherm model P310, Germany) with MoSi$_2$ resistors. The specimens were placed in a sintering bed of alumina powder for sintering. A heating rate of 1 °C/min was selected in the first (300 °C) and second (750 °C) firing stages with an isotherm plateau of 60 minutes in both stages, aiming

to eliminate the organic binder smoothly. Between 750 °C and 1600 °C, the heating rate was 5 °C/min, with a final densification plateau at 1600°C for 2h (120 minutes). After sintering, the samples were cooled at a 5 °C/min rate. The sintered samples were ground with grinding paper with SiC (#180→#320→#600) and polished with diamond polishing paste in a sequence of 15 µm→9µm→6µm→3µm→1µm. To determine the resistance to hydrothermal degradation, polished sintered samples of all compositions were submitted to aging by thermal cycle (15 min/cycle). It was carried out in an Autoclave Vitale Class 12L, at 134 ± 2 °C, pressure 216 kPa (2.2 kgf/cm), for 4 accumulated hours, with distilled water as a liquid medium. Previous studies have indicated that the exposition in an autoclave at 134 °C for 1 h is similar to exposition in body temperature for 3–4 years, so the simulated exposure time in the human body will be equivalent to 12 - 16 years[10,30].

### 2.2. Characterizations

The apparent density was measured using a SHIMADZU AUY220 precision electronic scale, applying the Archimedes method according to the recommendations of the ASTM C 373-14 standard[31]. The relative density was calculated by correlating the apparent density with the theoretical density of the compositions obtained by the mixture rule. The crystalline phases in the raw materials and in the sintered samples were identified by X-ray diffraction using a Panalytical model MRD PRO diffractometer, with Co-kα radiation, 40 KV power, and 40 mA current. The diffraction data were collected using an angular step of 0.02º and an acquisition time of 100 s/step. The crystalline peaks of each diffractogram were identified by comparing with crystallographic pattern files contained in the database of inorganic crystallographic structures (ICSD - Institute FIZ Karlsruhe-Leibniz): a) Al$_2$O$_3$–hexagonal (Space group R-3c) (ICSD#9771); b) ZrO$_2$-tetragonal (Space group P42/nmc) (ICSD#66786); c) ZrO$_2$-monoclinic (Space group P121/c1), d) CeO$_2$ -cubic (Space group R-3c). Furthermore, Rietveld refinement was carried out using the Full-Prof Suite program.

The microstructures of the sintered samples were evaluated using scanning electron microscopy (SEM) with a JEOL JSM 7100 F microscope. In this characterization step, two different analyses were adopted: The sintered samples were thermally etched at 1500 °C - 15 min to determine the compositional distribution of grains (*IMAGE J* software), and fractographic analysis was carried out on the fracture surfaces of the samples subjected to fatigue tests.

**Table 1.** Specifications of the starting powders used in this investigation (Manufacturer's data).

| Designation | Alumina CT3000LS (Alcoa Group, USA) | ZirPro® Intense ( Saint Gobain, France) |
|---|---|---|
| **Al$_2$O$_3$ (wt.%)** | 99.88 | 25 ± 1 |
| **ZrO$_2$ (wt.%)** | - | 64.5 |
| **CeO$_2$ /Y$_2$O$_{3 (95/5)}$ (wt.%)** | - | 10.5 ± 0.5 |
| **SiO$_2$ + Fe$_2$O$_3$ + Na$_2$O (wt.%)** | <0.05 | <0.06 |
| **MgO (wt.%)** | 0.04 | - |
| **Density (g/cm³)** | 3.98 | 5.56 |
| **Average Grain Size (µm) D50** | 0.5 | 0.2 |

The sintered samples were submitted to Vickers microhardness tests, following the recommendations of ASTM C 1327 - 15[32]. For statistical reasons, 25 Vickers impressions were made on the polished surfaces using a load of 2000 gF (9.8N) for 30s. The Emco Test model DuraScan 20 microhardness tester was used in this step. Fracture toughness was estimated using data generated in Vickers hardness tests. To analyze the type of crack system acting during crack growth, the model proposed in Equation 10 was used for monolithic and composite $Al_2O_3$ of group A and Equation 11 for the composite of group B, depending on the size of the observed cracks[33,34].

$$K_{IC} = 0.024.\left(\frac{E}{HV}\right)^{1/2}.\frac{P}{c^{3/2}} \quad \text{(System Palmqvist, } 0,25 \leq c/a \leq 2,5) \quad (10)$$

$$K_{IC} = 0.016.\left(\frac{E}{HV}\right)^{0,5}.\frac{P}{c^{3/2}} \quad \text{(System Half-penny, } c/a > 2,5) \quad (11)$$

Where, $K_{IC}$ = fracture toughness [MPa.m$^{1/2}$], $E$ = elastic modulus [GPa], $HV$ = Vickers hardness [GPa], $P$ = indentation load [MPa], "$a$" = semi diagonal of Vickers impression [m], "$l$" = crack length [m]; "$c$" = "$a + l$".

The elastic modulus of the sintered ceramics was measured by non-destructive acoustic testing using the Sonelastic IED model (São Carlos, Brazil) acoustic detection device.

## 2.3. Fatigue

Cyclic fatigue tests were carried out with four-point bending tests at room temperature and 60% relative humidity. The four-point bending test allows more reliable static or dynamic mechanical properties results than other tests such as three-point bending or biaxial bending (3P-B testing) due to the geometric configuration of the samples.

Four-point dynamic tests were performed using Landmark's Fatigue test machine model (MTS System Corporation, Minnesota, USA). Stresses in sinusoidal waves with a frequency of 15 Hz and a ratio of R = 0.2 were used. Samples with high fatigue life had their tests interrupted at $2 \times 10^6$ cycles, a value defined as run-out. Fatigue strength limits were determined using the modified staircase method. The technique's objective is to obtain at least one failure and one run-out for each sample. The preliminary value of stress amplitude used in the test was approximately 65% of the flexural strength of each material tested. If the specimen reached a number of cycles equivalent to the run-out without rupture, the stress level would be increased by one increment. In cases where the sample suffered a fracture in the cyclic test, a new specimen was tested at a stress level two increments below the one that caused the rupture, according to the guidelines for performing the method. It was necessary to guarantee the confidence that the stress values were above the chosen fatigue limit. Usually, the confidence level used is 90%. It means that if the tests are repeated, they will be above the calculated value with the chosen confidence level.

## 3. Results and Discussions

### 3.1. Physical and structural characterizations

The relative density values reported for the materials studied indicated relative density of the order of $98.5 \pm 0.6\%$

for the Control group (monolithic-$Al_2O_3$). The addition of Ce-ZTA powder provides discrete increases in densification among the groups of composites studied, $98.6 \pm 0.4\%$ and $99.1 \pm 0.7\%$ for composites with 5 wt.% or 20 wt.% Ce-ZTA addition, respectively.

Figures 1ab present X-ray diffractograms of the raw materials used in this study, and Figure 1c presents
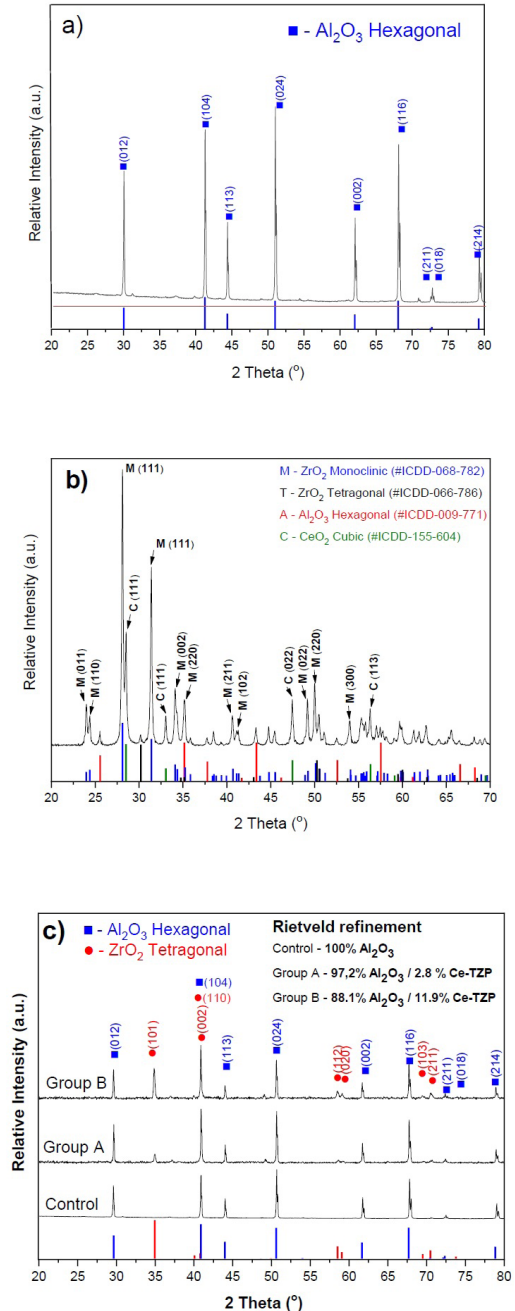


**Figure 1.** XRD patterns* of the starting powder and sintered samples: a) $Al_2O_3$ powder; b) $ZrO_2$-$Al_2O_3$-$CeO_2$ (Ce-ZTA) powder mixture; c) ceramics sintered at 1600°C-2h. * $Al_2O_3$–hexagonal (Space group R-3c) (ICSD#9771); $ZrO_2$ Tetragonal (Space group P42/nmc) (ICSD#66786); t-$ZrO_2$, m-$ZrO_2$ (Space group P121/c1), Cubic $CeO_2$ (Space group R-3c).

diffractograms of the different compositions after sintering at 1600 °C - 2h, after the hydrothermal degradation test, with the respective phase quantification results obtained by the Rietveld refinement of the sintered samples.
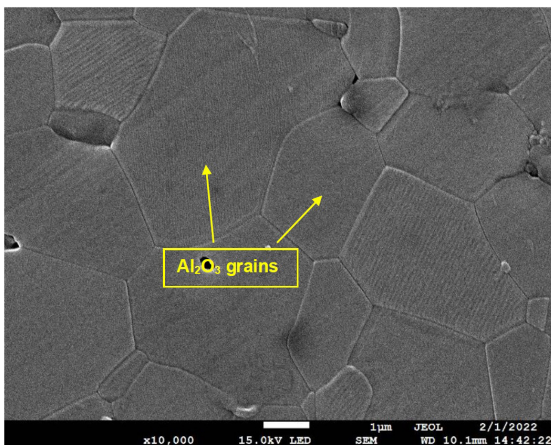
The Rietveld refinement results referring to Figure 1a indicated 100% $\alpha$−Al$_2$O$_3$ while the Ce-ZTA powder, Figure 1b, is composed of 64.5 wt.% monoclinic zirconia ($m$-ZrO$_2$), 0.9 wt.% of tetragonal zirconia ($t$-ZrO$_2$), 24.8 wt.% of $\alpha$−Al$_2$O$_3$, and 9.8 wt.% of cerium oxide, CeO$_2$. In addition, the analysis of the diffractograms of the sintered samples, Figure 1c, showed that regardless of the material analyzed, all groups present crystalline peaks of alumina (Al$_2$O$_3$) corresponding to the Al$_2$O$_3$-hexagonal structure. The composites sintered at 1600°C-2h showed 97.2 wt.% Al$_2$O$_3$+2.8wt.% $t$-ZrO$_2$ (Ce-TZP) for Group A, and 88.1 wt.% Al$_2$O$_3$ +11.9 wt.% Ce-TZP (Group B).

### 3.2. Microstructures

The sintered composite samples were thermally etched and analyzed by scanning electron microscopy for microstructural analysis. Figure 2 shows SEM micrographs of monolithic alumina samples composed of polygonal Al$_2$O$_3$ grains ranging in size from 1 μm and 3 μm.

Figure 3 shows the microstructure of sintered sample of Group B with polygonal grains of $\alpha$−Al$_2$O$_3$ and some ceria hexaluminate (H6A) platelets with a darker shade. The X-ray diffraction analysis did not detect this phase due to the low amount, lower than the detection limit of the diffractometer (3%). However, it has already been observed in previous works with the same raw material used in the present work[17]. The lighter grains are composed of the ceria-stabilized tetragonal zirconia (Ce-TZP) phase. The submicron Ce-TZP grains remain homogeneously dispersed at the triple points and the alumina grain boundaries. The primarily intergranular distribution of Ce-TZP grains was confirmed in an image obtained by compositional mapping by EDS, shown in Figure 4

As for sintered sample of Group A, the lower percentage of Ce-ZTA powder added to Al$_2$O$_3$ generated, after sintering, a smaller volumetric fraction of Ce-TZP grains well distributed

in the grain boundaries of the alumina matrix, as seen in Figure 5, obtained by backscattered electrons.

Previous works[35] have already identified residual stresses between the matrix and the intergranular phases during the cooling of sintered Al$_2$O$_3$ -ZrO$_2$ composites. For the composite
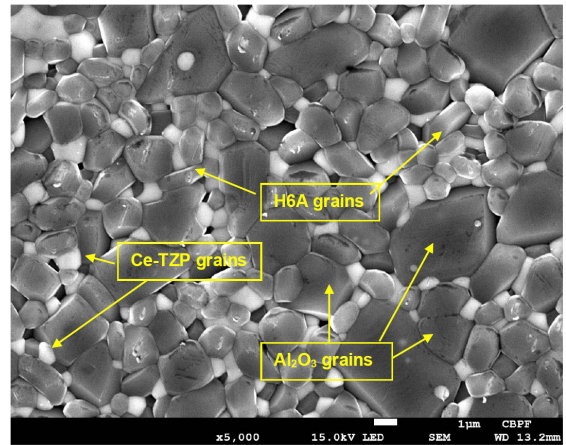


**Figure 3.** SEM micrograph of sample of Group B observing a matrix with polygonal Al$_2$O$_3$ grains, H6A alumina platelets, and lighter nanometric intergranular Ce-TZP grains. Magnification: 5000X.
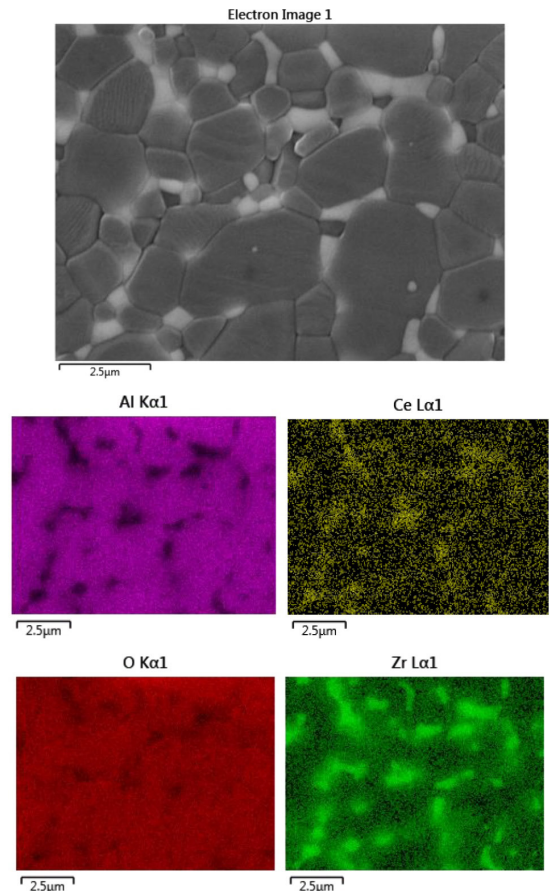


**Figure 4.** Compositional mapping of sample of Group B, showing the intergranular distribution of Ce and Zr elements, originating from Ce-TZP grains



**Figure 2.** Microstructure of sintered monolithic-alumina ceramic, containing polygonal $\alpha$-Al$_2$O$_3$ grains.

with the highest addition of Ce-ZTA, group B, the difference in thermal shrinkage between matrix and Ce-TZP grains after sintering may give rise to crack-like flaws or pore-like cavities. This effect is related to the crystallographic anisotropy between the two phases[35].

## 3.3. Mechanical properties

Figure 6 presents a summary of the mechanical properties evaluated in this work.

It can be seen in the graph that a correlation obtained by Rietveld refinement was made between the percentage of Ce-ZTA powder added in each composition and the ratio of Ce-TZP grains formed in the sintered sample in each case. Thus, the 5 wt.% Ce-ZTA powder composition generated the sintered specimen with 2.8 wt% Ce-TZP grains. The samples from group B (20 wt% Ce-ZTA powder) produced 11.9 wt% Ce-TZP grains. The average modulus of elasticity values obtained for monolithic alumina was 398 ± 15 GPa. As Ce-TZP was incorporated into the alumina
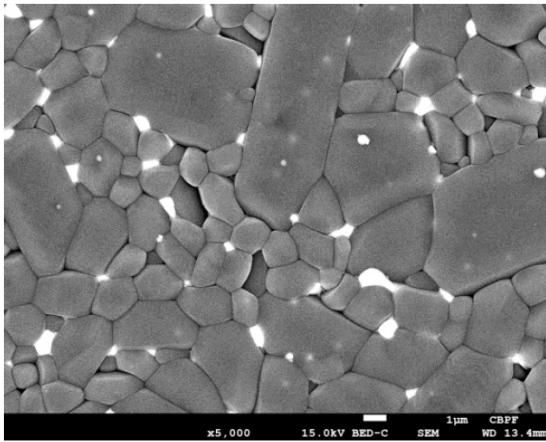


**Figure 5.** SEM micrograph of sintered sample of Group A, observing a smaller volumetric fraction of intergranular Ce-TZP grains (light grains) in the $Al_2O_3$-matrix compared to samples of Group B. (5000X magnification).
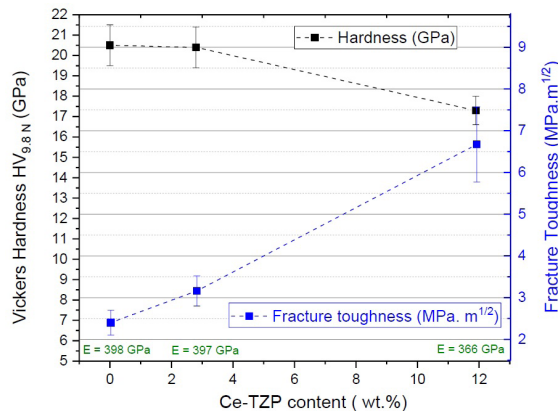


**Figure 6.** Hardness, fracture toughness, and modulus of elasticity (E) of the sintered $Al_2O_3$-samples as a function of Ce-TZP content.

matrix, a decrease in the average modulus of elasticity values was observed. This modulus for the highest levels of Ce-TZP (11.9 wt.%) values was 366 ± 34 GPa. Similarly, the addition of Ce-TZP reduced the Vickers hardness of alumina-based ceramics. The monolithic $Al_2O_3$ presented an average hardness of 20.5±1.0 GPa, while the group A ($Al_2O_3$ with 2.8 wt.% Ce-TZP) presented statistically similar average values of 20.4 ± 1.1 GPa. The presence of 11.9 wt.% Ce-TZP, in sintered samples of Group B, gave average values of 17.3 ± 0.7 GPa.

Observing the fracture toughness results of the different ceramic groups investigated, it is verified that the control group (100% $Al_2O_3$) has mean values of $K_{IC}$ = 2.4 ± 0.3 MPa.m$^{1/2}$, compatible with data reported in the literature[36]. Furthermore, the presence of a small amount of Ce-TZP grains observed in Group A produces a statistically significant increase in fracture toughness of this composite ($K_{IC}$ = 3.2 ±0.4 MPa.m$^{1/2}$), equivalent to 33% above that obtained in monolithic alumina. For group B, it was found that the fracture toughness presents a considerable increase, reaching average values of 6.7 ± 0.8 MPa.m$^{1/2}$. The presence of 11.9 wt.% Ce-TZP in the composition results in a significant 2.7-fold increase in material toughness compared to monolithic alumina (control group).

In ZTA (Zirconia-toughened alumina) composites, it is well established that the presence of the toughening phase composed of tetragonal zirconia has efficient toughening mechanisms, mainly toughening mechanism by $t{\rightarrow}m$ zirconia phase transformation[7,9]. This work demonstrates that the cerium-stabilized tetragonal zirconia grains, Ce-TZP, have an effective toughening capacity comparable to conventional yttria-stabilized zirconia, Y-TZP. The chemical configuration of the tetragonal structure using Ce and the consequent shielding zone at the crack tip of Ce-TZP systems are more intense and require higher energy levels than in Y-TZP ceramics for the $t{\rightarrow}m$ transformation to occur[7,9,16]. Thus, the increase in the amount of well-dispersed submicron Ce-TZP grains in the alumina matrix is primarily responsible for the considerable increase in fracture toughness observed in Group B. An additional benefit for the increase in fracture toughness observed using this powder mixture in this work (groups A and B) is the presence of secondary toughening mechanisms such as crack deflection, bridging, and pull-out, as observed in previous work[17], which occur due to the presence of alumina grains and low concentration of cerium hexaluminate platelets present in the composite, Figure 7, which consequently hinder crack growth[9,37-39].

An approximate calculation of the residual thermal stresses (tension and compression) resulting from the physical characteristics of both crystalline phases present in the composites, can be obtained by applying Equations 12, 13 and 14[40,41]:

$$\sigma_b = E_b \bullet \left( \alpha - \alpha_b \right) \bullet \Delta T \qquad (12)$$

$$\sigma_m = E_m \bullet \left( \alpha - \alpha_m \right) \bullet \Delta T \qquad (13)$$

$$\alpha = \frac{\alpha_b C_b E_b + \alpha_m C_m E_m}{C_b E_b + C_m E_m} \qquad (14)$$

Where, $\Delta T = 1575K$; $\sigma_b$ and $\sigma_m$ are the residual stresses in the Ce-TZP reinforcement and Al$_2$O$_3$ matrix, respectively. $E_b$ and $E_m$ indicate the Young's moduli of Ce-TZP (195 GPa) and Al$_2$O$_3$ (380 GPa), $C_m$ and $C_b$ corresponds to fraction of each phase and, $\alpha$, $\alpha_m$ and $\alpha_b$ indicate the coefficients of thermal expansion of the composite, the Al$_2$O$_3$ matrix (8.5 x 10$^{-6}$/°C) and Ce-TZP reinforcement (10.5 x 10$^{-6}$/ °C), respectively.

Applying these parameters, the theoretical values $\sigma_b$ = - 605 MPa and $\sigma_m$ = 17.9 MPa for group A and $\sigma_b$ = - 574 MPa and $\sigma_m$ = 78.4 MPa for group B. In both compositions, the set of compressive stresses acting on the Ce-TZP grains, As a result, stresses applied to Ce-TZP grains increase in composition containing higher Ce-TZP content (11.9 wt%), and under cyclic fatigue stresses, can lead to an acceleration of critical defects, in the composites of group B, requiring further studies for confirmation.

## 3.4. Fatigue

Table 2 presents the values of the fatigue strength limit of the ceramics obtained by the modified staircase method, and Figure 8 shows the experimental points obtained for the different compositions studied.

Fatigue strength values in brittle materials such as ceramics exhibit a large dispersion. Therefore, a statistical treatment was necessary to ensure the results' reliability. The method used for the calculations corrects the data obtained to provide confidence that the fatigue strength limit will be above the value found. In the present work, the estimated confidence is 90%. In Table 2, the fatigue strength limits of composites with the addition of Ce-ZTA powder showed higher values than
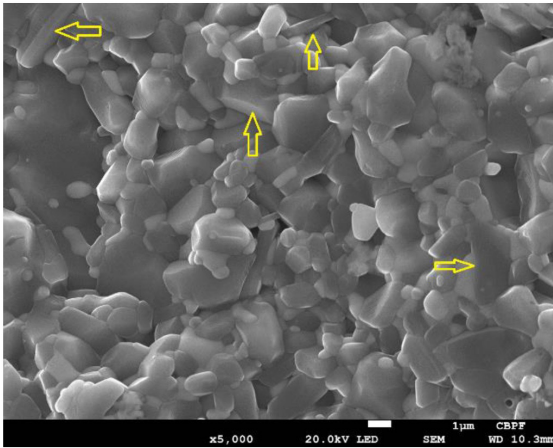


**Figure 7.** Fracture surface of sintered composite (Group B). *Sample showing Al$_2$O$_3$- matrix, Ce-TZP grains, and H6A alumina platelets (marked with yellow arrows). Magnification: 5000X.

those obtained for monolithic alumina. In these composites, the $t \rightarrow m$ transformation occurring in the Ce -TZP grains present at the triple points and grain boundaries during cyclic loading produces the crack tip shielding, an elastic constrained zone (zone shielding) that surrounds the crack tip. This phenomenon reduces the crack tip stress intensity factor and hinders crack growth[42], compared to monolithic alumina. Under cyclic loading conditions, the relationship between the stress intensity factors can be expressed on the microscale by Equations 12 and 13[42,43].

$$K_{tip} = K_I - K_S \tag{12}$$

$$\Delta K_{tip} = \Delta K - Ks \tag{13}$$

Where $K_{tip}$ and $\Delta K_{tip}$ are the stress intensity factor near the crack and the stress intensity range, respectively, $K_I$ is the nominal or applied stress intensity factor, and $\Delta K$ is the nominal or applied stress intensity range, given by $K_{max} - K_{min}$. $Ks$ is the intensity factor due to crack shielding[43].

Thus, adding Ce-ZTA powder to Al$_2$O$_3$ to produce the composites evaluated in this work promotes extrinsic toughening and the consequent increase in $Ks$. Among the composites (Groups A and B) tested under fatigue, the fatigue strength limit values are slightly lower for group B. The fatigue mechanisms for ceramic materials may depend on the material's microstructure. According to Murakami and Endo[44], heterogeneous materials contain inclusions and precipitates, which may have been added on purpose or from the manufacturing process. In turn, these inclusions and precipitates can directly affect the fatigue limit of the material. Therefore, once the crack starts at defects, the size of the crack produces the material boundary condition by intensifying the stress at the crack tip. Thus, some concepts of Murakami's theory define the fatigue strength limit as the limiting stress for the growth of cracks that have already started[44]. In the sintering of ceramic composites, the grains contract heterogeneously during cooling[45]. With the highest addition (20 wt.%) of Ce-ZTA in the Al$_2$O$_3$ matrix, group B (11.9 wt.% Ce-TZP) becomes more anisotropic and heterogeneous than group A (2.9% Ce-TZP). When an external load is applied to the sample, stresses are transmitted unevenly, focusing on failures or unstable grain boundaries[46,47]. It is observed in Table 2 that from group A to group B there was a decrease in the fatigue strength limit. The anisotropy and heterogeneity caused by the addition of Ce-ATZp in the composite of the present work were evidenced in the SEM images, Figures 3 to 5. Therefore, the fatigue strength limit may have been affected due to the degradation of grain bridging since the higher the content of Ce-TZP grains and some highly anisotropic H6A platelets in the Al$_2$O$_3$ matrix, the greater the heterogeneity of the composite.

**Table 2.** Fatigue strength limits ($\sigma$) with the Modified Staircase Method for monolithic alumina (control group) and composites (groups A and B).
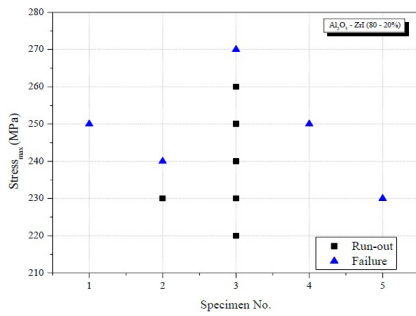
| Specimens | Composition (in wt.%) | $\sigma$(MPa) | Confidence Interval |
|---|---|---|---|
| Control Group | 100% $\alpha$-Al$_2$O$_3$ | 100 ± 14 | 90% |
| Group A | 97.2% $\alpha$-Al$_2$O$_3$ + 2.8% Ce-TZP | 279 ± 14 | 90% |
| Group B | 88.1% $\alpha$-Al$_2$O$_3$ + 11.9% Ce-TZP | 239 ± 32 | 90% |
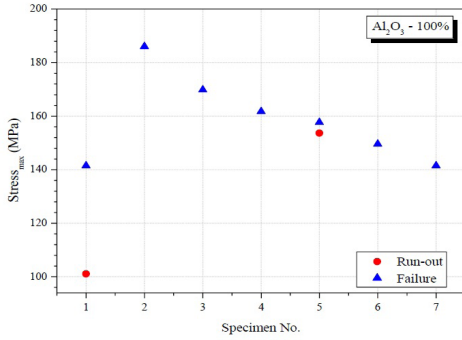
(a)
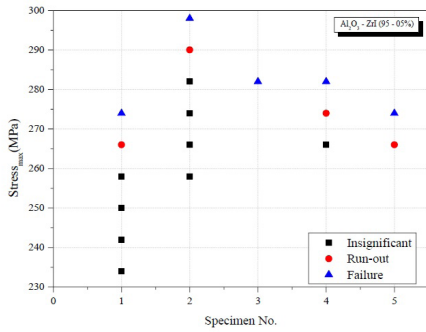


(b)



(c)

**Figure 8.** Experimental points obtained with the Modified Staircase Method to determine the fatigue strength limit: a) Control Group (monolithic-$Al_2O_3$); b) Group A; c) Group B.

## 3.5. *Failure analysis*

The fracture surfaces of the samples tested under fatigue were analyzed by scanning electron microscopy to determine the origin of the failure and microstructural aspects. Figure 9 presents images obtained on the fracture surfaces of composites (group A and group B) at lower magnifications so that the origin and propagation of the failure can be noted.

Despite having higher fracture toughness values, Group B presented a lower fatigue strength limit when compared to group A. Relevant research[48] examined new strategies for developing materials that efficiently solve toughness and strength conflicts. In the present work, all composites showed higher fracture toughness and fatigue strength limits than monolithic alumina. In this case, it is inferred that the addition of Ce-ZTA powder to the alumina allows, during sintering, the intergranular precipitation of Ce-TZP grains. During the cyclic fatigue test, the occurrence of the *tetragonal → monoclinic* transformation in these grains, present in the triple points and the grain boundaries, results in the crack tip shielding. Consequently, it causes the reduction of the crack tip stress intensity factor, delaying the growth of the cracking and increasing the fatigue strength limit. However, for higher addition of Ce-ZTA powder (20 wt%) in group B, the concentration of an appreciable volumetric fraction of Ce-TZP grains and the formation of an irregular surface at the grain boundaries of the alumina matrix occurs in the sintering, as observed on the fracture surface of the sample of this composition, tested under fatigue (Figure 10).

Figure 10 shows a predominant intergranular fracture, with Ce-TZP grains adhered to the surface and grain boundaries of the alumina matrix. The intergranular Ce-TZP grains, when in appreciable quantity, under excessive thermal stresses and containing microstructures containing grains with anisotropy of thermal expansion typical of hexagonal structures, domains, dislocations, are subject to possible inferences of possible microcracks that can act as stress concentrators in samples subjected to cyclic stresses, and form the thicker and rough grain boundary layer.

Furthermore, the differences in the thermal expansions between the alumina, H6A, and Ce-ATZ grains that occur in the sintering can promote the formation of microcracks in the intergranular region, which act as crack propagation
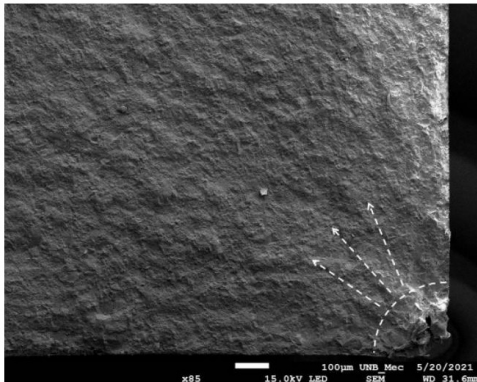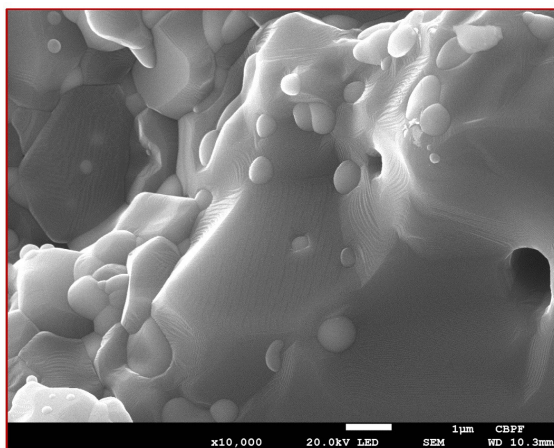


(a)
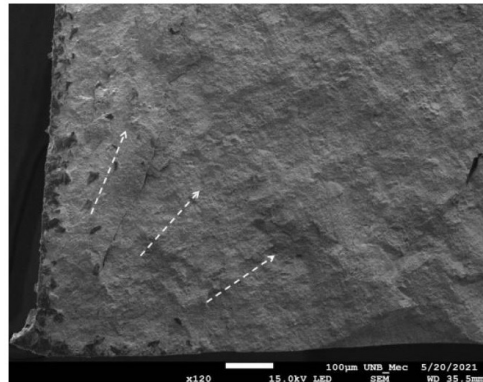


(b)

**Figure 9.** SEM micrographs of the fracture surfaces of ceramic composites after fatigue tests: a) Group A; (b) Group B.

**Figure 10.** SEM Micrograph of the fracture surface of the sample of group B with larger grains belonging to the alumina matrix and smaller grains of Ce-TZP.

regions, reducing fatigue strength. Therefore, it is inferred that in samples of group B, the addition of 20wt% of Ce-ATZp formed weaker grain boundaries and led to a decrease in the grain boundary bonding strength compared to composition A. Consequently, we observed lower values of fatigue strength limits with the increase of the additive content for the composites evaluated in this work.

## 4. Conclusions

The $Al_2O_3$-ceramic composites revealed high relative density improved with the progressive addition of Ce-TZP in the composition, which showed high resistance to hydrothermal degradation. In addition, the fracture toughness values indicated that the Ce-TZP grains were effective for toughening due to the $t{\rightarrow}m$ transformation mechanism consistent with the typical shielding characteristics at the crack tip around the Ce-TZP grains.

Compared to monolithic-$Al_2O_3$ (control group), which presented a fatigue strength limit of 100 MPa, in sintered composites, the occurrence of the $t{\rightarrow}m$ transformation that occurs in Ce -TZP grains present at the triple points and grain boundaries during cyclic loading produces an elastic constrained zone (zone shielding) that surrounds the crack tip. This phenomenon leads to a reduction in the crack tip stress intensity factor and retards crack growth when compared to monolithic-$Al_2O_3$. However, with the reinforcing increase (group B), the Ce-TZP grains present a higher volumetric fraction (11.9%), forming the thicker and rough grain boundary layers and acting as stress concentrators. In addition, the differences in the thermal expansions between the alumina and Ce-ATZ grains that occur in the sintering promote the formation of microcracks in the intergranular region.

It is inferred, therefore, that, despite both composites having fatigue strength limits superior to monolithic-$Al_2O_3$, the increase in the concentration of Ce-TZP grains presented in group B formed weaker grain boundaries and led to a decrease in the grain boundary bonding strength, when compared to group A. Consequently, we observed lower

values of fatigue strength limits with increasing additive content for the composites evaluated in this work.

## 6. References

1. Dörre E, Hubner H. Alumina: processing, properties, and applications. Berlin, Germany: Springer; 1984.
2. Huet R, Sakona A, Kurtz SM. Review - Strength and reliability of alumina ceramic femoral heads: review of design, testing, and retrieval analysis. J Mech Behav Biomed Mater. 2011;4(3):476-83.
3. Ruys AJ. Alumina ceramics: biomedical and clinical applications. Oxford: Woodhead Publishing; 2019.
4. Punj S, Singh J, Singh K. Ceramic biomaterials: properties, state of the art and future prospectives. Ceram Int. 2021;47(20):28059-74.
5. Sommer F, Landfried R, Kern F, Gadow R. Mechanical properties of zirconia toughened alumina with 10-24 vol.% 1.5 mol% Y-TZP reinforcement. J Eur Ceram Soc. 2012;32(15):3905-10.
6. Zadorozhnaya OY, Khabas TA, Kamyshnaya KS, Kutugin VA, Malykhin SE. Effects of sintering curves on microstructure, physical and mechanical properties and on low-temperature degradation of zirconia-toughened alumina. J Eur Ceram Soc. 2021;41:274-81.
7. Basu B. Toughening of yttria-stabilized tetragonal zirconia ceramics. Int Mater Rev. 2005;50(4):239-56.
8. Chevalier J, Gremillard L, Virkar AV, Clarke DR. The tetragonal-monoclinic transformation in zirconia: lessons learned and future trends. J Am Ceram Soc. 2009;92(9):1901-20.
9. Kelly PM, Rose LF. The martensitic transformation in ceramics: its role in transformation toughening. Prog Mater Sci. 2002;47(5):463-557.
10. Chevalier J, Cales B, Drouin JM. Low-temperature aging of Y-TZP ceramics. J Am Ceram Soc. 1999;82:2150-4.
11. Rose LRF, Swain MV. Transformation zone shape in ceria partially-stabilized zirconia. Acta Metall. 1988;36(4):955-62.
12. Rauchs G, Fett T, Munz D, Oberacker R. Tetragonal-to-monoclinic phase transformation in $CeO_2$-stabilised zirconia under uniaxial loading. J Eur Ceram Soc. 2001;21(12):2229-41.
13. Gogotsi GA, Zavada VP, Swain MV. Characterization of a 9 mol% Ce-TZP ceramic material - I. Flexual response. J Eur Ceram Soc. 1995;15:1185-92.
14. Cutler RA, Mayhew RJ, Prettyman KM, Virkar AV. High-toughness Ce-TZP/$Al_2O_3$ ceramics with improved hardness and strength. J Am Ceram Soc. 1991;74(1):179-86.
15. Tsai J-F, Belnap JD, Shetty DK. Crack shielding in Ce-TZP/$Al_2O_3$ composites: comparison of fatigue and sustained load crack growth specimens. J Am Ceram Soc. 2005;77(1):105-17.
16. Nawa M, Yamada K, Kurizoe N. Effect of the t–m transformation morphology and stress distribution around the crack path on the measured toughness of zirconia ceramics: a case study on Ce-TZP/alumina nanocomposite. J Eur Ceram Soc. 2013;33:521-9.
17. Santos C, Coutinho IF, Amarante JEV, Alves MFRP, Coutinho MM, Silva CRM. Mechanical properties of ceramic composites based on $ZrO_2$ co-stabilized by $Y_2O_3$–$CeO_2$ reinforced with $Al_2O_3$ platelets for dental implants. J Mech Behav Biomed Mater. 2021;116:104372.
18. Kern F. A comparison of microstructure and mechanical properties of 12Ce-TZP reinforced with alumina and *in situ* formed strontium- or lanthanum hexaaluminate precipitates. J Eur Ceram Soc. 2014;34(2):413-23.

19. Kern F, Gommeringer A. Reinforcement mechanisms in yttria-ceria-Co-stabilized zirconia alumina-strontium hexaaluminate composite ceramics. J Ceram Sci Techn. 2018;9(1):93-8.

20. Kern F. Properties of 2 mol% yttria stabilized zirconia–alumina–cerium hexaaluminate composites. Ceramics. 2020;3(2):190-8.

21. CIMAC: International Council on Combustion Engines. IACS UR M53, appendix IV: guidance for evaluation of Fatigue Tests [Internet]. 2009 [cited 2022 Apr 14]. Available from: https://www.jicef.org/pdf_cimac/pdf_cimac_general/CIMAC_WG4_AppendixIV.pdf

22. Lee Y-LEA. Fatigue testing and analysis. Burlington, USA: Elsevier; 2005.

23. Lin S, Lee Y, Lu M. Evaluation of the staircase and the accelerated test methods for fatigue limit distribution. Int J Fatigue. 2001;23:75-83.

24. Lee Y, Pan J, Hathaway RB, Barkey ME. Fatigue test and analysis: theory and practice. Burlington: Elsevier Butterworth–Heinemann; 2005.

25. ASTM: American Society for Testing and Materials. ASTM E739-15: standard practice for statistical analysis of linear or linearized stress-life (S-N) and strain-life (ε-N) fatigue data. West Conshohocken: ASTM International; 2018.

26. Machado PVS, Araújo LC, Soares MV, Reis L, Araújo JA. Multiaxial fatigue assessment of steels with non-metallic inclusions by means of adapted critical plane criteria. Theor Appl Fract Mech. 2020;108:102585.

27. Souza RC, Santos C, Barboza MJR, Bicalho LA, Baptista CAP, Elias CN. Fatigue behavior of 3%$Y_2O_3$-doped $ZrO_2$ ceramics. J Mater Res Technol. 2014;3(1):48-54.

28. Zhang J, Zhu T, Sang S, Li Y, Pan L, Liao N, et al. Microstructural evolution and mechanical properties of $ZrO_2$(3Y)–$Al_2O_3$–SiC(w) ceramics under oscillatory pressure sintering. Mater Sci Eng A. 2021;819:141445.

29. Scherrer SS, Cattani-Lorente M, Vittecoq E, Mestral F, Griggs JA, Wiskott HWA. Fatigue behavior in water of Y-TZP zirconia ceramics after abrasion with 30μm silica-coated alumina particles. Dent Mater. 2011;27(2):e28-42.

30. Burlington DB. Steam re-sterilization causes deterioration of zirconia ceramic heads of total hip prostheses. Washington, DC: Food and Drug Administration; 1997.

31. ASTM: American Society for Testing and Materials. ASTM C373-14: Standard test method for water absorption, bulk density, apparent porosity, and apparent specific gravity of fired whiteware products, ceramic tiles, and glass tiles. West Conshohocken: ASTM International; 2014.

32. ASTM: American Society for Testing and Materials. ASTM C1327-15: standard test method for vickers indentation hardness of advanced ceramics. West Conshohocken: ASTM International; 2019.

33. Casellas D, Nagl MM, Llanes L, Anglada M. Fracture toughness of alumina and ZTA ceramics: microstructural coarsening effects. J Mater Process Technol. 2003;143-144:148-52.

34. Niihara K. A fracture mechanics analysis of indentation-induced palmqvist crack in ceramics. J Mater Sci Lett. 1983;2:221-3.

35. Ma Q, Pompe W, French JD, Clarke DR. Residual stresses in $Al_2O_3$-$ZrO_2$ composites: a test of stochastic stress models -. Acta Metall Mater. 1994;42(5):1673-81.

36. Ćurković L, Rede V, Grilec K, Lalić M. Determining the fracture toughness of alumina ceramics from vickers indentations. Mater Test. 2009;51(1):199-202.

37. Kern F, Gadow R. In situ platelet reinforcement of alumina and zirconia matrix nanocomposites - one concept, different reinforcement mechanisms. AST. 2014;87:118-25.

38. Gregori G, Burger W, Sergo V. Piezo-spectroscopic analysis of the residual stress in zirconia-toughened alumina ceramics: the influence of the tetragonal-tomonoclinic transformation. Mater Sci Eng. 1999;A27:401-6.

39. Fan K, Ruiz-Hervias J, Pastor JY, Gurauskis J, Baudin C. Residual stress and diffraction line-broadening analysis of $Al_2O_3$/Y-TZP ceramic composites by neutron diffraction measurement. Int J Refract Met Hard Mater. 2017;64:122-34.

40. Shi JL, Lu ZL, Guo JK. Model analysis of boundary residual stress and its effect on toughness in thin boundary layered yttria-stabilized tetragonal zirconia polycrystalline ceramics. J Mater Res. 2000;15(3):727-32.

41. Shi JL, Li L, Guo JK. Boundary stress and its effect on toughness in thin boundary layered and particulate composites: model analysis and experimental test on Y-TZP-based ceramic composites. J Eur Ceram Soc. 1998;18(14):2035-43.

42. Ritche RO. Mechanisms of fatigue crack propagation in metals, ceramics, and composites: role of crack tip shielding. Mater Sci Eng A. 1988;103:15-28.

43. Chevalier J, Olagnon C, Fantozzi G. Crack propagation and fatigue in zirconia-based composites. Compos, Part A Appl Sci Manuf. 1999;30:525-30.

44. Murakami Y, Endo M. Effects of defects, inclusions and inhomogeneities on fatigue strength. Int J Fatigue. 1994;16:163-82.

45. Daniel R, Meindlhumer M, Baumegger W, Juraj T, Zalesak J, Ziegelwanger T, et al. Anisotropy of fracture toughness in nanostructured ceramics controlled by grain boundary design. Mater Des. 2019;101:80-5.

46. Kirchner HP, Gruver RM. Strength-anisotropy-grain Size relations in ceramic oxides. J Am Ceram Soc. 1970;53:232-6.

47. Maca K, Pouchly V, Drdlik D, Hadraba H, Chlup Z. Dilatometric study of anisotropic sintering of alumina/zirconia laminates with controlled fracture behavior. J Eur Ceram Soc. 2017;37(14):4287-95.

48. Ritchie R. The conflicts between strength and toughness. Nat Mater. 2011;10:817-22.